Brain changes within the visuo-spatial attentional network in posterior cortical atrophy

Chiara Cerami[a,b], MD, Chiara Crespi [a], MSc, Pasquale Anthony Della Rosa [a,c], PhD, Alessandra Dodich[a], MSc, Alessandra Marcone [b], MD, Giuseppe Magnani [d], MD, Elisabetta Coppi [d], MD, Andrea Falini[a,e], MD, Stefano F. Cappa [g], MD, and Daniela Perani [a,c,f], MD.

a) Università Vita-Salute San Raffaele, Milan, Italy
b) Clinical Neuroscience Department, San Raffaele Hospital, Milan, Italy
c) Istituto di Bioimmagini e Fisiologia Molecolare C.N.R., Segrate, Italy
d) Department of Neurological, Institute of Experimental Neurology–INSPE, San Raffaele Hospital, Milan, Italy
e) Department of Neuroradiology, CERMAC, San Raffaele Hospital, Milan, Italy
f) Department of Nuclear Medicine, Division of Neuroscience, San Raffaele Hospital, Milan, Italy
g) Istituto Universitario di Studi Superiori, Pavia, Italy

Word Count:228 abstract and 3292 text

Tables, Figures: 1 table and 2 figures; 1 Table on Supplementary Materials

Running Title: [^{18}F]FDG-PET and MRI study in PCA

Corresponding Author:

Dr. Chiara Cerami

Università Vita-Salute San Raffaele and ClinicalNeuroscience Dept., San Raffaele Hospital

Via Olgettina 60 – 20134 Milan (Italy)

Tel. 02 26435760 – 2713

Fax. 02 26435738

e-mail: cerami.chiara@hsr.it

Abstract

Posterior Cortical Atrophy (PCA) is characterized by basic visual and high order visual-spatial dysfunctions. In this study, we investigated long-distance deafferentation processes within the frontal-parietal-occipital network in ten PCA patients using a MRI-PET combined approach. Objective voxel-based [^{18}F]FDG-PET imaging measured metabolic changes in single patients. Comprehensive investigation of Diffusion Tensor Imaging (DTI) metrics and grey-matter density with Voxel-based Morphometry (VBM) were obtained in a subgroup of 6 patients. Fractional anisotropy (FA) in the superior longitudinal fasciculus correlated with the PET metabolic changes within the inferior parietal and frontal eye field regions. [^{18}F]FDG-PET analysis showed in each PCA case the typical bilateral hypometabolic pattern, involving posterior temporal, parietal, and occipital cortex, with additional hypometabolic foci in the frontal eye fields. VBM showed right-sided atrophy in the parieto-occipital cortex**,** as well as a limited temporal involvement. DTI revealed extensive degeneration of the major anterior-posterior connecting fiber bundles and of commissural frontal lobe tracts. Microstructural measures in the superior longitudinal fasciculus were correlated with the PET metabolic changes within the inferior parietal and frontal eye field regions. Our results confirmed the predominant occipital-temporal and occipital-parietal degeneration in PCA patients. [^{18}F]FDG-PETand DTI-MRI combined approaches revealed neurodegeneration effects well beyond the classical posterior cortical involvement, most likely as a consequence of deafferentation processes within the occipital-parietal-frontal network that could be at the basis of visuo-perceptual, visuo-spatial integration and attention deficits in PCA.

Keywords: [^{18}F]FDG-PET Imaging, Voxel-Based Morphometry, Diffusion Tensor Imaging, Dementia, Posterior Cortical Atrophy, Frontal Eye Field.

Introduction

Posterior cortical atrophy (PCA) is a clinico-radiological syndrome currently considered among the atypical presentation of Alzheimer's disease (AD). No definite epidemiological data are available, but mean age at disease onset appears to be earlier than in typical AD (i.e., 50-65 years old) [1]. Although its main pathological features are those of AD, as suggested by amyloid PET imaging studies [2-3], the PCA phenotype may reflect other pathological substrates, not linked to AD pathology [1]. The disorder is characterized by a progressive degeneration involving, in particular, posterior occipital brain areas, mainly affecting high order visuo-spatial processing. High order visuo-spatial and visuo-perceptual disorders, as well as impairments of basic visual processing are the core features [1,4]. The combination of these symptoms reflects the damage to specific cortical regions, including the primary visual cortex, as well as neural streams processing different types of visual information (i.e., parietal or dorsal stream, occipito-temporal or ventral stream). In addition, affected patients may present alexia, features of Balint and/or Gerstmann syndromes [4], and progressive oral language dysfunctions with prominent word retrieval difficulties, compatible with the logopenic/phonological variant of primary progressive aphasia [5-6], reflecting extension of disease to the parietal and temporal cortex.

Only a few structural and functional neuroimaging studies investigated the specific patterns of grey- and white-matter damage, together with metabolic changes in PCA patients. Cross-sectional voxel-based morphometry (VBM) and cortical thickness measures showed a bilateral pattern of atrophy, predominant in the right hemisphere, in occipital, parietal and posterior temporal lobes, compared to healthy subjects [7-9]. In comparison with AD patients, the PCA group presented a greater involvement of right visual associative cortex [9]. Diffusion tensor imaging (DTI) studies showed fractional anisotropy (FA) alterations, supporting a reduction of the microstructural integrity of long white-matter tracts connecting posterior regions [10-12]. A follow-up report in a patient with 3 years of symptom duration showed an early FA reduction in the occipital white

matter, followed after 15 months by more widespread white-matter damage extending to the parietal lobe [13].

More limited evidence comes from [^{18}F]fluorodeoxyglucose-positron emission tomography (FDG-PET) and SPECT studies of PCA patients at the group level, which indicated prevalent metabolic changes in the parieto-occipital areas (right worse than left) [14-16]. In a [^{18}F]FDG-PET study, the frontal eye field regions were found to be hypometabolic, suggesting loss of input from occipito-parietal regions [17]. Noteworthy, neuroanatomical and perfusion dysfunctions of a large fronto-parietal network in the right hemisphere accounted for the presence of left-sided neglect in PCA patients [18].

In this study, we investigated the neuroanatomical substrate as well as the regional cerebral hypometabolism in a sample of PCA patients. VBM and DTI group analysis was used to assess grey- and white-matter damage, whereas an objective voxel-based analysis of [^{18}F]FDG-PET data was applied to assess metabolic changes at both the single-subject and group level. We hypothesized the presence of a correlation between the microstructural changes within the anterior-posterior connecting fiber tracts, in particular the superior longitudinal fasciculus, and the metabolic changes extending anteriorly to the frontal eye field regions. This may be attributed to reduced input from occipito-parietal regions and contribute to the core clinical symptoms.

Material and Methods

Subjects

Ten PCA patients (8 women, 2 men; mean age = 65.54±5.25 years; mean education = 12.4±4; mean months from symptoms' onset = 43.7±10.6; mean Mini Mental State Examination (MMSE) = 16.6±4.8) were consecutively enrolled in the study (Table 1). All patients were referred to San Raffaele Hospital (Milan, Italy) complaining of an insidious onset of visual deficits in absence of ocular disorders. Patients were evaluated by a team of experienced behavioral neurologists and

neuropsychologists. The diagnosis was based on clinical history, neurological evaluation, neuropsychological assessment, and neuroimaging findings [1,19-20]. In particular, all patients presented with the insidious onset and gradual progression of basic and complex visual disorders in the absence of ophthalmologic alterations or other neurological conditions at CT/MR imaging. In comparison to visual disorders, memory loss and other cognitive impairments were significantly less prominent in the clinical picture.

A long disease course was reported in all patients (months' from symptoms onset range = 28-60), which had generally referred first to opticians and ophthalmologists for their visual problems, resulting in a delay in the clinical diagnosis. Basic visual deficits (i.e., hemianopia) were shown at the neurological examination in 7 out of 10 patients. No patient showed fluctuations of cognition, visual hallucinations or extrapyramidal signs, i.e. core features for the diagnosis of possible or probable dementia with Lewy bodies (DLB) [21]. No patient reported family history.

Conventional structural imaging (i.e., Magnetic Resonance Imaging (MRI) or Computed Tomography (CT)) showed widespread posterior brain atrophy in all cases, mostly involving occipital and parietal lobes. Posterior temporal atrophy was present in four out of ten patients. Seven patients showed also small nonspecific T2 hyperintensities in the subcortical white matter.

Clinical evaluation and instrumental data including neuropsychological assessment and neuroimaging (i.e., VBM and DTI brain MRI and cerebral [^{18}F]FDG-PET) were collected within few weeks. Neuropsychological assessment was performed by expert neuropsychologists focusing also on areas of selective impairment [11]. In particular, global cognitive functioning (Mini Mental State Examination); memory function (Rey Auditory Verbal Learning Test; Rey's figure recall test); executive functions (verbal and visual digit span task); language functions (phonological and semantic fluency; Token test; Aachener Aphasie Test (AAT) or "Batteria per l'analisi dei deficit afasici" (BADA) subtests); visuo-perceptual and visuo-spatial deficits (Rey's figure copy test and Visual Object and Space Perception Battery (VOSP) subtests). Object and face recognition tests were also administered as well as apraxia and finger agnosia tests.

All subjects, or their informants/caregivers, gave informed consent to the experimental procedures that had been approved by the local Ethical Committee.

MRI data acquisition and analysis

MRI scans were acquired in 6 out of 10 patients (i.e., from #1 to #6 on Table 1; 4 women, 2 men; mean age = 64.9±3.6 years; mean education = 12±4.3; mean months from symptoms' onset = 38.8±7.3; mean MMSE = 17±6.3) using a 3-T Philips Achieva scanner (Philips Medical Systems, Best, NL) with an 8-channel head coil. The resulting data set was compared with 20 healthy age-matched controls (HC) (mean age = 60±9.3 years; mean education = 13±4.2; mean MMSE = 29.25±0.78). Scanning session included T1-weighted volumetric MR scan (220 slices, TR/TE=600/20 ms, voxel size 0.9x0.9x0.8 mm^3) and a single-shot echo planar sequence (TR/TE=8986/80 ms; FOV=240 mm^2; 56 sections; 2.5 mm isotropic resolution) with parallel imaging (SENSE factor, R=2.5) and diffusion gradients applied along 32 non-collinear directions (b-value=1000 s/mm2). Four out of the ten patients of whole PCA sample dropped out from this part of the study due to presence of pacemaker, refusal or claustrophobia.

VBM pre-processing and statistical analyses were performed using SPM8 (http://www.fil.ion.ucl.ac.uk/spm) on Matlab v7.4 (Mathworks-Inc., Sherborn, MA), along with the VBM8 (http://dbm.neuro.uni-jena.de) and Diffeomorphic Anatomical Registration Through Exponentiated Lie algebra (DARTEL) toolboxes, according to what previously reported [22]. The non-linear modulated DARTEL normalized GM images were smoothed with a 8-mm Full-Width-Half-Maximum (FWHM) Gaussian-kernel and used in the subsequent voxel-based statistical analyses to compare patient GM volume with 20 age- and education-matched healthy controls.The statistical threshold was set at $p < 0.05$ Family-wise-Error (FWE) corrected for multiple comparisons either at the voxel-level or at the cluster-level and the voxels extent threshold was set at k=100. Cerebral regions showing significant effects were localized using the SPM-Anatomy toolbox v1.

Pre-processing and analysis of DTI data were performed via the FMRIB Software Library (FSL) tools (http://fsl.fmrib.ox.ac.uk/fsl/fslwiki/). Whole-brain group analysis on main diffusion invariants (i.e., fractional anisotropy (FA), mode of anisotropy (MO) [23], mean diffusivity (MD), axial diffusivity (AxD), and radial diffusivity (RD)) were carried out via Tract-Based Spatial Statistics (TBSS) [24]. Group comparisons were conducted via *Randomise,* setting the significance threshold for group differences at $p<0.05$, according to what reported in a previous study [25].

To exclude gender effects, we added participant gender as a nuisance covariate in both studies.

[^{18}F]FDG-PET data acquisition and analysis

[^{18}F]FDG-PET acquisitions were performed in all patients at the Nuclear Medicine Unit, San Raffaele Hospital (Milan, Italy). Before radiopharmaceutical injection of [^{18}F]FDG (185–250 Mbq: usually, 5-8 mCi via a venous cannula), subjects were fasted for at least 6 hours and measured blood glucose level threshold was <120 mg/dL. All images were acquired with a Discovery STE (GE Medical Systems, Milwaukee, WI) multi-ring PET tomography (PET-CT) system (time interval between injection and scan start = 45 minutes; scan duration = 15 minutes). Images were reconstructed using an ordered subset expectation maximization (OSEM) algorithm. Attenuation correction was based on CT scan. Specific software integrated in the scanner was used for scatter correction. Subjects' scans were obtained at resting state in a relaxed and comfortable position. All subjects gave written informed consent, following detailed explanation of the [^{18}F]FDG-PET procedure.

Image pre-processing was performed using SPM statistical parametric mapping (http://www.fil.ion.ucl.ac.uk/spm/software) according to the procedure implemented in the new standardized SPM5 [^{18}F]FDG dementia-specific template [26] for spatial normalization of [^{18}F]FDG-PET scans of dementia patients. This is an optimized method that showed increased reliability and accuracy of estimated metabolic activity patterns compared to the standard [^{15}O]H_2O-PET template currently available for SPM normalization procedures [26]. Indeed, it allows to better

recognize relevant metabolic changes that otherwise may be suppressed through spatial normalization.Images were smoothed with a 8-mm Full-Width-Half-Maximum (FWHM) Gaussian-kernel. Proportional scaling was used to remove intersubject global variation in PET intensities, according to Signorini and co-workers [27].

Each patient scan was tested for relative 'hypometabolism' by comparison with a large sample of [^{18}F]FDG-PET scans from a database of normal controls (n=112) on a voxel-by-voxel basis. Healthy controls were selected by the European Alzheimer Disease Consortium (EADC)-PET dataset (http://www.eadc.info/).Cognitive health was established in each EADC-PET center by means of a structured clinical and a neuropsychological battery as specified in a previous paper [28]. Age was included in the two sample T-test analysis as a covariate. Due to the lack of any significant difference in metabolic activity of male and female Alzheimer patients [29], gender was not controlled in the analysis. The threshold was set at p=0.05, FWE-corrected for multiple comparisons at the voxel level. Only clusters containing more than 100 voxels were deemed to be significant. In each subject, cerebral regions showing significant hypometabolism were identified using the SPM-Anatomy toolbox v1.

In order to compute brain metabolic changes at the group level, we performed a second-level SPM analysis (one-sample T-test) in the whole PCA group. The threshold was set at p=0.05, FWE-corrected for multiple comparisons at the cluster level.

Finally, to explore the study hypothesis, we correlated (i.e., Spearman rank order correlation coefficient)metabolic values obtained from a set of 8-mm ROIs, including regions that are crucial components of the fronto-parietal attentional network, and mean values of main diffusion tensor metrics (i.e., FA, MO, MD, RD, AxD) extracted from portions of the bilateral Superior Longitudinal Fasciculus (SLF) found to be affected in patients *vs.* controls (PCA<HC) in the whole-brain TBSS comparison. Our [^{18}F]FDG-PET single-subject analysis revealed indeed the involvement of frontal as well as parietal eye field regions (see result section). These hypometabolic foci revealed by [^{18}F]FDG-PET SPM analysis in single subjects strictly corresponded to the

stereotactic coordinates from functional PET and fMRI literature (i.e., bilateral frontal eye fields (i.e., middle frontal gyrus/precentral sulcus and superior frontal gyrus/superior frontal sulcus) [30-31], right intraparietal sulcus [32-33] and left inferior parietal lobe [31]). Thus, we used the above stereotactic coordinates to center the ROIs. Correlation p-values were adjusted for multiple comparisons with the False Discovery Rate (FDR) correction [34].

Results

In PCA patients, the clinical and neuropsychological assessment at presentation revealed mostly visuo-perceptual and visuo-spatial disorders variably associated to features of Balint's and/or Gerstmann's syndromes (e.g., oculomotor apraxia, optic ataxia, environmental agnosia, acalculia, agraphia, finger agnosia), alexia, anomia or ideomotor apraxia. Episodic memory impairment was present in 8 out of 10 patients at standard neuropsychological evaluation (i.e., Rey Auditory Verbal Learning Test). See Table 1 for clinical and neuropsychological details.

In PCA group compared to HC, VBM whole-brain analysis of grey-matter volume revealed an right-sided atrophy in the occipital (fusiform gyrus, middle occipital gyrus, and lingual gyrus) and parietal (cuneus and precuneus) regions and in the inferior temporal gyrus; a small area of atrophy was evident in the left fusiform gyrus (Figure 1A). Globally, TBSS analyses on main diffusion invariants in PCA patients compared to HC showed widespread microstructural changes ($p<0.05$, FWE-corrected) in the major association bundles connecting occipital, parietal, temporal and frontal regions (i.e., inferior fronto-occipital fasciculus (IFOF), superior longitudinal fasciculus (SLF), inferior longitudinal fasciculus (ILF), uncinate fasciculus (UF), cingulum bundle and fornix), as well as the commissural tracts and projections fibers (i.e., splenium and thalamic radiations). In particular, statistical maps of FA (PCA<HC), MD (PCA>HC) and RD (PCA>HC) (Figure 2) demonstrated a bilateral pattern of microstructural alterations, mainly affecting the right-sided circuitry, more severely involving the posterior portions of association bundles, as well as the

forceps major, the body and the splenium of the corpus callosum. The latter finding has been considered as one of the core features of the PCA [35]. In addition, we found the involvement of commissural frontal lobe tracts, i.e. the genu of corpus callosum and the forceps minor. Both the AxD (PCA>HC) and the MO (PCA<HC) maps showed a selective involvement of long fibers of the right hemisphere (Figure 2).

Objective-based SPM [^{18}F]FDG-PET single-subject analysis showed a consistent pattern of temporo-parietal hypometabolism, typical of AD [36]. In addition, we found a core feature of bilateral hypometabolism in the occipital cortex, mostly involving associative visual areas and in few cases also the primary visual cortex (see Figure 3 and Table 1 on Supplementary Materials). All patients showed also unilateral or bilateral involvement of middle frontal gyrus/precentral sulcus and/or superior frontal gyrus/superior frontal sulcus, comparable to what was found in a previous [^{18}F]FDG-PET group study on PCA patients (i.e., left superior/medial frontal gyrus BA 6/8 (x, y, z = -28, 12, 46), and right (x, y, z = 30, 18, 42; 34, 8, 46 and 27, 42, 24) and left (x, y, z = -28, 40, 28) medial frontal gyrus [17]). These regions are associated to the visuomotor and oculomotor control [37-39]. In particular, they belong to the classical location of the human frontal eye fields (FEF) (i.e., medial frontal gyrus in the proximity of the precentral sulcus) [37] the supplementary eye fields (i.e., superior/superior medial frontal gyrus) [39].

The group analysis of [^{18}F]FDG-PETusing SPM procedures showed a bilateral temporo-parietal (right>left) hypometabolism, comparable to the well-known AD pattern, and an additional widespread hypometabolism of the occipital cortex, mainly of the associative visual regions (p=0.05, FWE-corrected for multiple comparisons at the cluster level). At a lower statistical threshold of significance (p=0.05 uncorrected; k = 100 voxels of minimum extent), an additional cluster of hypometabolism corresponding to the right frontal eye field region was present(k =271 voxels, T = 2.80; MNI coordinates of local maxima x,y,z = 30,10,62) (Figure 1B).

Correlation analysis showed significant association between hypometabolism in fronto-parietal regions and FA along the SLF in the right hemisphere. In particular, the mean diffusion tensor

metrics derived from altered clusters of the right SLF was correlated with hypometabolism values extracted from the ROIs in the right precentral gyrus (ρ_{FA}=-0.94, p=0.012; ρ_{MD}=0.94, p=0.012; ρ_{RD}=-0.89, p=0.031; ρ_{AxD}=0.82, p=0.05 FDR-corrected) (x, y, z = 50, 2, 53) [30], encompassing the right frontal eye field [36] and with hypometabolism values extracted from the ROIs in the right intraparietal sulcus (ρ_{FA}=-0.88, p=0.025 FDR-corrected) (x, y, z = 39, -36, 42) [33], which is involved in visuo-spatial integration and attention, and classically considered as the parietal eye field [38].

Neither hypometabolism in the regions of interest nor mean FA values along the SLF correlated with the overall cognitive impairment (i.e., MMSE), and disease duration (i.e., months from symptoms onset).

Discussion

Misdiagnosis or diagnostic delay of PCA is common, because of its relative rarity and of its variable presentation. Patients are frequently first seen by an ophthalmologist, who may correctly note the normal eye examinations but fail to appreciate the clinical evidence of cortical dysfunction [1]. Although neuroimaging has a relevant role in corroborating the clinical diagnosis [40], specific structural and/or functional features to be applied in the clinical practice, at single-subject level, are in the course of definition [41].

In this study, we showed, in a group of PCA subjects, MRI structural changes in posterior cortical regions, namely in the parieto-occipital areas, which are consistent with previous works [7-9] (see Figure 1A).

The voxel-based SPM analysis of [^{18}F]FDG-PET data, at the group level, confirmed the well-known posterior bilateral hypometabolic pattern suggestive of AD, with the additional specific involvement of the occipital lobes, in agreement with other reports in literature and with the pathological substrate of PCA syndrome [14,17] (see Figure 1B). The metabolic derangement of the

occipital cortex was independent of disease duration. The cerebral hypometabolism, since it reflects various underlying mechanisms, such as deafferentation and neuronal injury processes, was more extended that the atrophy pattern revealed by the VBM results.

In addition, at a lower statistical threshold, the [^{18}F]FDG-PET group analysis revealed also the functional damage of the right frontal eye field region. This finding was particularly evident at the single-subject level. SPM analysis of [^{18}F]FDG PET scans provided in individuals evidence for a diffuse pattern of bilateral occipito-temporal and occipito-parietal hypometabolism, mostly lateralized to the right side. Noteworthy, it disclosed additional hypometabolic foci in the frontal eye fields, i.e. regions involved in the eye movement control [37-39], consistent with the hypometabolic findings reported by Nestor and co-workers in their group analysis [17] (see Figure 3 and Table 2 on the Supplementary Materials). Thus, [^{18}F]FDG-PET SPM analysis revealed both at the group and at the single-subject level the dysfunction of frontal regions that are involved in the preparation and triggering of intentional saccades, in pursuit eye movements and in the control of memory-guided saccades, particularly in case of spatial memory tasks [4,39]. These regions are also crucial components of the fronto-parietal attentional network, and are richly connected with posterior parietal cortex by means of recurrent fibers passing through the superior longitudinal fasciculus [42]. This network is extensively damaged in PCA patients, resulting in a reduction/interruption of the input to the frontal lobe, as confirmed also by our DTI-PET correlation results. A disruption of this complex network may be responsible for the visuomotor disorders, such as oculomotor and optic ataxia, which have been frequently reported in PCA [1,4,18] (see Table 1).

This specific [^{18}F]FDG-PET hypometabolic pattern was associated to DTI findings of extensive white-matter microstructural degeneration in long associative bundles, thus reflecting deafferentation processes between posterior parieto-occipital regions and anterior frontal structures (see Figure 2 and 3).This is the first DTI study providing a comprehensive view of the microstructural changes in PCA with evidence in the main diffusion invariants (i.e., FA, MD, AxD, RD and MO). In comparison to previous studies [10-12], we showed more widespread white-matter

degeneration in long associative bundles connecting the occipital cortices and the parietal and temporal regions. In particular, a severe alteration of diffusion orientation coherence in PCA patients – reflected by an extensive FA reduction involving the posterior and anterior components of major associative bundles – was also accompanied by a significant decrease of MO in the right hemisphere, which indicates a transition from a more linear to more planar shape of the diffusion tensor [23]. Taken together these findings highlight the presence of a severe and extensive disorganization of white-matter microstructural architecture in PCA patients, further supported by the co-localized alterations in MD, AxD/RD maps. Indeed, while the relevant increase in MD indicates an overall alteration in the rate of the diffusion, which is thought to reflect the neurodegeneration process [43], changes observed in AxD and RD maps are suggestive of more specific axonal damages in terms of axon density/loss and breakdown in axon integrity [44].

Noteworthy, such an extensive pattern of damage includes both ventral (e.g., ILF and IFOF) and dorsal (e.g., SLF) pathways in both hemispheres, with the right-sided circuitry appearing more prominently impaired. A major involvement of the right hemisphere is a typical feature of the neurodegeneration in PCA, already reported in the literature [7-9], reflecting a specific vulnerability of still unknown origin. Again, the decrease in MO may suggest a more severe microstructural disorganization of the right-sided fiber tracts

, and the significant alteration in the AxD index an incipient breakdown in axon integrity. Consequently, the bilateral pattern of microstructural alteration in PCA observed in FA, MD and RD maps may also be hypothesized to reflect a possible spread of the pathological processes from the right to the left hemisphere.

The alterations observed in the SLF and ILF/IFOF bundles, which are crucial to convey visual perceptual and spatial information to anterior brain areas [45], may be conceivably caused either by wallerian degeneration due to either neuronal loss or by the presence of senile plaques and neurofibrillary tangles in occipito-parieto-temporal regions [1] affecting as a consequence both structural and functional brain connectivity. The decrease of white-matter integrity found in the

commissural fibers, including the forceps major and the splenium of the corpus callosum – i.e., a key-feature of the PCA – may also reflect a secondary degenerative process resulting from the pathological disruption of occipital, parietal and temporal neurons, as previously suggested by Yoshida et al. [35].

Overall, microstructural white matter alterations observed in PCA patients mirror their cognitive profile, which encompasses broad deficits in perceptual and visuospatial skills, and are the basis for the disconnection and dysfunction as revealed by [^{18}F]FDG PET. Of note, the altered connectivity along the dorsal stream conveyed by the SLF, and particularly by the second branch might result in a reduction/interruption of the input to the frontal lobe, producing the attention deficits and the neglect occasionally observed in PCA [46]. Such visuospatial deficits are indeed related to intra-hemispheric functional imbalances, involving large-scale fronto-parietal pathways [18].

In conclusion, notwithstanding the relatively small size of the patient sample, this study contributes to further characterize the selective vulnerability of specific brain networks in PCA, describing for the first time DTI microstructural changes in all main diffusion invariants, and an anterior-posterior metabolic dysfunction in each case, providing evidence of the fronto-parietal disconnection within the visuo-spatial attentional network. Furthermore, this specific PET metabolic pattern detected at a single subject level may aid the differential diagnosis with other dementia subtypes, such as DLB or typical AD. Typical AD cases present with a relative sparing of occipital lobes on [^{18}F]FDG-PETscan, and DLB patients usually with a more extended decrease of metabolic activity in parieto-temporo-occipital regions, and also in frontal associative cortex, together with metabolic increases in subcortical regions (e.g., thalamus and pons) [36,47]. An improved definition of the neuroimaging pattern of the PCA syndrome may be useful in the definition of new, biomarker-based diagnostic criteria [41].

Acknowledgment including sources of support: This study was supported by the Italian Ministry of Health [RICERCA FINALIZZATA 2008 Conv 12, Sponsor Protocol Number 09/2011

Molecular Imaging; Molecular imaging for the early diagnosis and monitoring of Alzheimer's disease in old individuals with cognitive disturbances: an ADNI- compatible prospective Study, EudraCT number 2011-004415-24] and by EU FP7 INMIND Project (FP7-HEALTH-2011-two-stage “Imaging of Neuroinflammation in Neurodegenerative Diseases”, grant agreement no. 278850). Dr. Cerami was funded by Fondazione Eli-Lilly [Eli-Lilly grant 2011 "Imaging of neuroinflammation and neurodegeneration in prodromal and presymptomatic Alzheimer's disease phases"].

Disclosure statement for authors: No actual or potential conflicts of interest to disclose.

References

[1] Crutch SJ, Lehmann M, Schott JM, Rabinovici GD, Rossor MN, Fox NC (2012) Posterior cortical atrophy. *Lancet Neurol***11**(2), 170-178.

[2] Formaglio M, Costes N, Seguin J, Tholance Y, Le Bars D, Roullet-Solignac I, Mercier B, Krolak-Salmon P, Vighetto A (2011) In vivo demonstration of amyloid burden in posterior cortical atrophy: a case series with PET and CSF findings. *J Neurol***258**, 1841-1851.

[3] Rosenbloom MH, Alkalay A, Agarwal N, Baker SL, O'Neil JP, Janabi M, Yen IV, Growdon M, Jang J, Madison C, Mormino EC, Rosen HJ, Gorno-Tempini ML, Weiner MW, Miller BL, Jagust WJ, Rabinovici GD (2011) Distinct clinical and metabolic deficits in PCA and AD are not related to amyloid distribution. *Neurology***76**, 1789-1796.

[4] Shakespeare TJ, Yong KX, Frost C, Kim LG, Warrington EK, Crutch SJ (2013) Scene perception in posterior cortical atrophy: categorization, description and fixation patterns. *Front Hum Neurosci* 2013 Oct 2; **7**, 621.

[5] Crutch SJ, Lehmann M, Warren JD, Rohrer JD (2013) The language profile of posterior cortical atrophy. *J Neurol Neurosurg Psychiatry***84**(4), 460-466.

[6] Magnin E, Sylvestre G, Lenoir F, Dariel E, Bonnet L, Chopard G, Tio G, Hidalgo J, Ferreira S, Mertz C, Binetruy M, Chamard L, Haffen S, Ryff I, Laurent E, Moulin T, Vandel P, Rumbach L (2013). Logopenic syndrome in posterior cortical atrophy. *J Neurol***260**(2), 528-533.

[7] Lehmann M, Crutch SJ, Ridgway GR, Ridha BH, Barnes J, Warrington EK, Rossor MN, Fox NC (2011) Cortical thickness and voxel-based morphometry in posterior cortical atrophy and typical Alzheimer's disease. *Neurobiol Aging***32**, 1466-1476.

[8] Lehmann M, Barnes J, Ridgway GR, Ryan NS, Warrington EK, Crutch SJ, Fox NC (2012) Global gray matter changes in posterior cortical atrophy: a serial imaging study. *Alzheimers Dement***8**(6): 502-512.

[9] Whitwell JL, Jack CR Jr, Kantarci K, Weigand SD, Boeve BF, Knopman DS, Drubach DA, Tang-Wai DF, Petersen RC, Josephs KA (2007) Imaging correlates of posterior cortical atrophy. *Neurobiol Aging*. **28**(7), 1051-1061.

[10] Migliaccio R, Agosta F, Rascovsky K, Karydas A, Bonasera S, Rabinovici GD, Miller BL, Gorno-Tempini ML (2009) Clinical syndromes associated with posterior atrophy: early age at onset AD spectrum *Neurology***73(**19), 1571-1578.

[11] Migliaccio R, Agosta F, Toba MN, Samri D, Corlier F, de Souza LC, Chupin M, Sharman M, Gorno-Tempini ML, Dubois B, Filippi M, Bartolomeo P (2012) Brain networks in posterior cortical atrophy: a single case tractography study and literature review. *Cortex***48**(10), 1298-1230.

[12] Migliaccio R, Agosta F, Scola E, Magnani G, Cappa SF, Pagani E, Canu E, Comi G, Falini A, Gorno-Tempini ML, Bartolomeo P, Filippi M (2012) Ventral and dorsalvisualstreams in posteriorcorticalatrophy: A DT MRI study. *Neurobiol Aging***33,** 2572-2584.

[13] Duning T, Warnecke T, Mohammadi S, Lohmann H, Schiffbauer H, Kugel H, Knecht S, Ringelstein EB, Deppe M (2009) Pattern and progression of white-matter changes in a case of posterior cortical atrophy using diffusion tensor imaging. *J Neurol Neurosurg Psychiatry***80**, 432-436.

[14] Schmidtke K, Hüll M, Talazko J (2005) Posterior cortical atrophy: variant of Alzheimer's disease? A case series with PET findings. *J Neurol***252**(1), 27-35.

[15] Kas A, de Souza LC, Samri D, Bartolomeo P, Lacomblez L, Kalafat M, Migliaccio R, Thiebaut de Schotten M, Cohen L, Dubois B, Habert MO, Sarazin M (2011) Neural correlates of cognitiveimpairment in posterior cortical atrophy. *Brain***134**, 1464-1478.

[16] Andrade K, Kas A, Samri D, Sarazin M, Dubois B, Habert MO, Bartolomeo P (2013) Visuospatial deficits and hemispheric perfusion asymmetries in posterior cortical atrophy. *Cortex***49**(4), 940-947.

[17] Nestor PJ, Caine D, Fryer TD, Clarker J, Hodges JR (2003) The topography of metabolic deficits in posterior cortical atrophy (the visual variant of Alzheimer's disease) with FDG-PET. *J Neurol Neurosurg Psychiatry***74**(11), 1521-1529.

[18] Andrade K, Kas A, Valabrègue R, Samri D, Sarazin M, Habert MO, Dubois B, Bartolomeo P, (2012) Visuospatial deficits in posterior cortical atrophy: structural and functional correlates. *J Neurol Neurosurg Psychiatry***83**(9), 860-863.

[19] Alladi S, Xuereb J, Bak T, Nestor P, Knibb J, Patterson K, Hodges JR (2007) Focal cortical presentations of Alzheimer's disease. *Brain***130**(10), 2636-2645.

[20] McMonagle P, Deering F, Berliner Y, Kertesz A (2006) The cognitive profile of posterior cortical atrophy. *Neurology***66**(3), 331-338.

[21] McKeith IG, Dickson DW, Lowe J, Emre M, O'Brien JT, Feldman H, Cummings J, Duda JE, Lippa C, Perry EK, Aarsland D, Arai H, Ballard CG, Boeve B, Burn DJ, Costa D, Del Ser T, Dubois B, Galasko D, Gauthier S, Goetz CG, Gomez-Tortosa E, Halliday G, Hansen LA, Hardy J, Iwatsubo T, Kalaria RN, Kaufer D, Kenny RA, Korczyn A, Kosaka K, Lee VM, Lees A, Litvan I, Londos E, Lopez OL, Minoshima S, Mizuno Y, Molina JA, Mukaetova-Ladinska EB, Pasquier F, Perry RH, Schulz JB, Trojanowski JQ, Yamada M and Consortium on DLB (2005) Diagnosis and management of dementia with Lewy bodies: third report of the DLB Consortium. *Neurology***65**(12), 1863-1872.

[22] Cerami C, Dodich A, Canessa N, Crespi C, Iannaccone S, Corbo M, Lunetta C, Consonni M, Scola E, Falini A, Cappa SF (2013) Emotional empathy in amyotrophic lateral sclerosis: a behavioural and voxel-based morphometry study. *Amyotroph Lateral Scler Frontotemporal Degener* 2013 Apr 16. [Epub ahead of print].

[23] Ennis DB, Kindlmann G (2006) Orthogonal Tensor Invariants and the Analysis of Diffusion Tensor Magnetic Resonance Images. *Magn Reson Med***55**, 136-146.

[24] Smith SM, Jenkinson M, Johansen-Berg H, Rueckert D, Nichols TE, Mackay CE, Watkins KE, Ciccarelli O, Cader MZ, Matthews PM, Behrens TE (2006) Tract-based spatial statistics: voxelwise analysis of multi-subject diffusion data. *Neuroimage* **31,** 1487-1505.

[25] Crespi C, Cerami C, Dodich A, Canessa N, Arpone M, Iannaccone S, Corbo M, Lunetta C, Scola E, Falini A, Cappa SF (2014) Microstructural white matter correlates of emotion recognition impairment in Amyotrophic Lateral Sclerosis. *Cortex* 2014 Jan 18 [Epub ahead of print].

[26] Della Rosa PA, Cerami C, Gallivanone F, Prestia A, Castiglioni I, Gilardi MC, Friston K, Ashburner J, Perani D, and the EADC-PET Consortium (2014) A New Standardized [^{18}F]-FDG-PET Template for Spatial Normalization in Statistical Parametric Mapping Analysis of Brain Images in Dementia. *Neuroinformatics* in press.

[27] Signorini M, Paulesu E, Friston K, Perani D, Colleluori A, Lucignani G, Grassi F, Bettinardi V, Frackowiak RS, Fazio F. (1999) Rapid assessment of regional cerebral metabolic abnormalities in single subjects with quantitative and nonquantitative [^{18}F]FDG PET: a clinical validation of statistical parametric mapping. *NeuroImage***9,** 63-80.

[28] Morbelli S, Drzezga A, Perneczky R, Frisoni GB, Caroli A, van Berckel BN, Ossenkoppele R, Guedj E, Didic M, Brugnolo A, Sambuceti G, Pagani M, Salmon E, Nobili F (2012) Resting metabolic connectivity in prodromal Alzheimer's disease. A European Alzheimer Disease Consortium (EADC) project.*Neurobiol Aging***33**, 2533-2550.

[29] Minoshima S, Giordani B, Berent S, Frey KA, Foster NL, Kuhl DE (1997) Metabolic reduction in the posterior cingulate cortex in very early Alzheimer's disease. *Ann Neurol***42**, 85-94.

[30] Gagnon D, O'Driscoll GA, Petrides M, Pike GB (2002) The effect of spatial and temporal information on saccades and neural activity in oculomotor structures. *Brain***125**(Pt 1), 123-139.

[31] Doricchi F, Perani D, Incoccia C, Grassi F, Cappa SF, Bettinardi V, Galati G, Pizzamiglio L, Fazio F (1997) Neural control of fast-regular saccades and antisaccades: an investigation using positron emission tomography. *Exp Brain Res***116**(1), 50-62.

[32] Bray S, Arnold AE, Iaria G, MacQueen G (2013) Structural connectivity of visuotopic intraparietal sulcus. *Neuroimage***82**, 137-145.

[33] Daw ND, O'Doherty JP, Dayan P, Seymour B, Dolan RJ (2006) Cortical substrates for exploratory decisions in humans. *Nature***441**, 876-879.

[34] Yoav B & Hochberg Y (1995) Controlling the false discovery rate: a practical and powerful approach to multiple testing. *Journal of the Royal Statistical Society. Series B (Methodological),* vol. **57**, No.1, pp. 289-300.

[35] Yoshida T, Shiga K, Yoshikawa K, Yamada K, Nakagawa M (2004) White matter loss in the splenium of the corpus callosum in a case of posterior cortical atrophy: a diffusion tensor imaging study. *Eur Neurol***52**, 77-81.

[36] Teune LK, Bartels AL, de Jong BM, Willemsen AT, Eshuis SA, de Vries JJ, van Oostrom JC, Leenders KL (2010) Typical cerebral metabolic patterns in neurodegenerative brain diseases. *Mov Disord*. **25**(14), 2395-2404.

[37] Paus T (1996) Location and function of the human frontal eye-field: a selective review. *Neuropsychologia***34**(6), 475-483.

[38] Pierrot-Deseilligny C, Milea D, Müri RM (2004) Eye movement control by the cerebral cortex. *Curr Opin Neurol***17**(1), 17-25.

[39] Tehovnik EJ, Sommer MA, Chou IH, Slocum WM, Schiller PH (2000) Eye fields in the frontal lobes of primates. *Brain Res Brain Res Rev*. **32**(2-3), 413-448.

[40] Tsai PH, Teng E, Liu C, Mendez MF (2011) Posterior cortical atrophy: evidence for discrete syndromes of early-onset Alzheimer's disease. *Am J Alzheimers Dis Other Demen***26,** 413-418.

[41] Crutch SJ, Schott JM, Rabinovici GD, Boeve BF, Cappa SF, Dickerson BC, Dubois B, Graff-Radford NR, Krolak-Salmon P, Lehmann M, Mendez MF, Pijnenburg Y, Ryan NS, Scheltens P, Shakespeare T, Tang-Wai DF, van der Flier WM, Bain L, Carrillo MC, Fox NC. (2013) Shining a light on posterior cortical atrophy. *Alzheimers Dement***9**(4), 463-465.

[42] Ptak R (2012) The frontoparietal attention network of the human brain: action, saliency, and a priority map of the environment. *Neuroscientist***18**(5), 502-515.

[43] Beaulieu C. (2002) The basis of anisotropic water diffusion in the nervous system–a technical review. *NMR in Biomedicine* **15**(7-8), 435-455.

[44] Bennett IJ, Madden DJ, Vaidya CJ, Howard DV, Howard JH Jr. (2010) Age- related differences in multiple measures of white matter integrity: A diffusion tensor imaging study of healthy aging. *Human brain mapping* **31**(3), 378-390.

[45] Goodale MA, Milner AD (1992) Separate visual pathways for perception and action. *Trends Neurosci***15**, 20-25.

[46] Thiebaut de Schotten M, Tomaiuolo F, Aiello M, Merola S, Silvetti M, Lecce F, Bartolomeo P, Doricchi F (2014) Damage to white matter pathways in subacute and chronic spatial neglect: a group study and 2 single-case studies with complete virtual "in vivo" tractography dissection. *Cereb Cortex* 2014 Mar; **24**(3), 691-706. Epub 2012 Nov 15.

[47] Minoshima S, Foster NL, Sima AA, Frey KA, Albin RL, Kuhl DE (2001) Alzheimer's disease versus dementia with Lewy bodies: cerebral metabolic distinction with autopsy confirmation. *Ann Neurol***50**(3), 358-365.

Table 1. Demographic data and clinical-neuropsychological features of PCA patients. Raw score are provided. N.t. = not testable; n.a. = not available; * = patient's refusal. Scores under the cut-off are shown in bold.

	#1	#2	#3	#4	#5	#6	#7	#8	#9	#10
Demographic data										
Age (years)	63	63	69	67	59	67	77	65	64	59
Gender	M	F	M	F	F	F	F	F	F	F
Education	13	10	18	13	13	5	13	8	18	13
Clinical features										
Months from symptoms' onset	32	48	33	48	36	36	48	36	60	60
Environmental agnosia	+	+	+	+	+	-	+	-	+	+
Visual fields disorders (i.e., hemianopia)	+	+	-	+	+	-	-	+	+	+
Oculomotor apraxia and optic ataxia	-	+	-	+	-	+	-	+	-	-
Visuo-perceptual deficits	+	+	+	+	+	+	+	+	+	+
Visuo-spatial deficits	+	+	+	+	+	+	+	+	+	+
Visuo-spatial memory deficits	+	+	+	+	+	+	+	+	+	+
Alexia	-	+	+	+	-	-	+	+	+	+
Agraphia	+	+	+	+	+	-	-	-	-	+
Ideomotor apraxia	-	-	-	+	+	+	+	-	-	+
Anomia	+	-	+	+	-	+	-	-	+	-
Prosopagnosia	-	+	-	+	+	-	-	-	-	+
Episodic memory deficits	+	-	+	+	+	+	-	+	+	+
Other(e.g., acalculia, finger agnosia)	-	+	+	-	+	+	-	-	-	+
Neuropsychological assessment										
MMSE	22	22	16	15	20	17	17	17	14	16
Forward digit span	5	5	5	3	6	5	4	6	4	4
Backward digit span	**3**	**2**	**3**	**3**	**3**	**2**	**2**	**3**	**3**	**2**
Corsi block-tapping test	**2**	**2**	**2**	**2**	**2**	**2**	**2**	**2**	**3**	*
Attentive Matrices	**22**	**15**	**27**	**n.t.**	**11**	**6**	**8**	**n.t.**	**17**	**9**
RAVLT Immediate Recall	**15**	38	**15**	**15**	**23**	**21**	28	**11**	**19**	**10**

RAVLT Delayed Recall	**0**	6	**1**	**0**	**0**	**2**	6	**1**	**2**	**3**
Category fluency	25	23	**13**	**11**	**13**	20	**13**	**9**	**17**	**14**
Fonemic fluency	17	34	**5**	**5**	**8**	20	24	**17**	21	24
Token test	30	**23**	**20**	**n.t.**	**22**	**25**	**23**	**n.t.**	**18**	**24**
AATdenomination	n.a.	106/120	**60/120**	n.a.	**57/120**	**54/120**	n.a.	n.a.	n.a.	n.a.
AATоral comprehension	n.a.	60/60	60/60	n.a.	n.a.	59/60	n.a.	n.a.	n.a.	n.a.
Rey figure copy	**0.5**	**4**	**13.5**	**6.5**	**0.5**	**2**	**2.5**	**7.5**	**4.5**	*
Rey figure recall	**0**	**4.5**	7	**0**	**0**	**2**	**0**	**3.5**	n.a.	*
Constructional Apraxia Test	8	**2**	**8**	**2**	**2**	**0**	**0**	**2**	**0**	**0**
Raven's Progressive Matrices	**11**	**14**	20	**n.t.**	**n.t.**	**7**	**n.t.**	**n.t.**	**n.t.**	**n.t.**
VOSP Object perception Screening test	**n.t.**	18/20	18/20	**n.t.**	**n.t.**	**n.t.**	**n.t.**	**n.t.**	**n.t.**	**n.t.**
Incomplete letters		**6/20**	17/20							
Silhouettes		**8/30**	19/30							
Object decision		18/20	16/20							
Progressive Silhouettes		10/20	**12/20**							
Space perception Dot counting		**2/10**	**7/10**							
Position discrimination		**12/20**	**17/20**							
Number Location		**4/10**	9/10							
Cube analysis		**1/10**	**3/10**							
Finger Agnosia	n.a.	**11/24**	**13/24**	n.a.	**10/24**	**8/24**	n.a.	n.a.	n.a.	**12/24**

Figure Legend:

Figure 1. A) Voxel-based morphometry group maps (VBM-MRI) ($p<0.05$, FWE corrected) displayed on render and axial (x=3) views of an MRI standardized structural scan, showing GM reduction in right occipital-parietal and temporal regions and more limited cluster on the left fusiform gyrus. B) Voxel-based [^{18}F]FDG-PET group analysis showing extended bilateral temporo-parietal-occipital (right>left) hypometabolism, and additional hypometabolic foci on the right frontal eye field. Results are displayed on render view of an MRI standardized structural scan ($p=0.05$ uncorrected; k = 100 voxels of minimum extent) L = left; R = right.

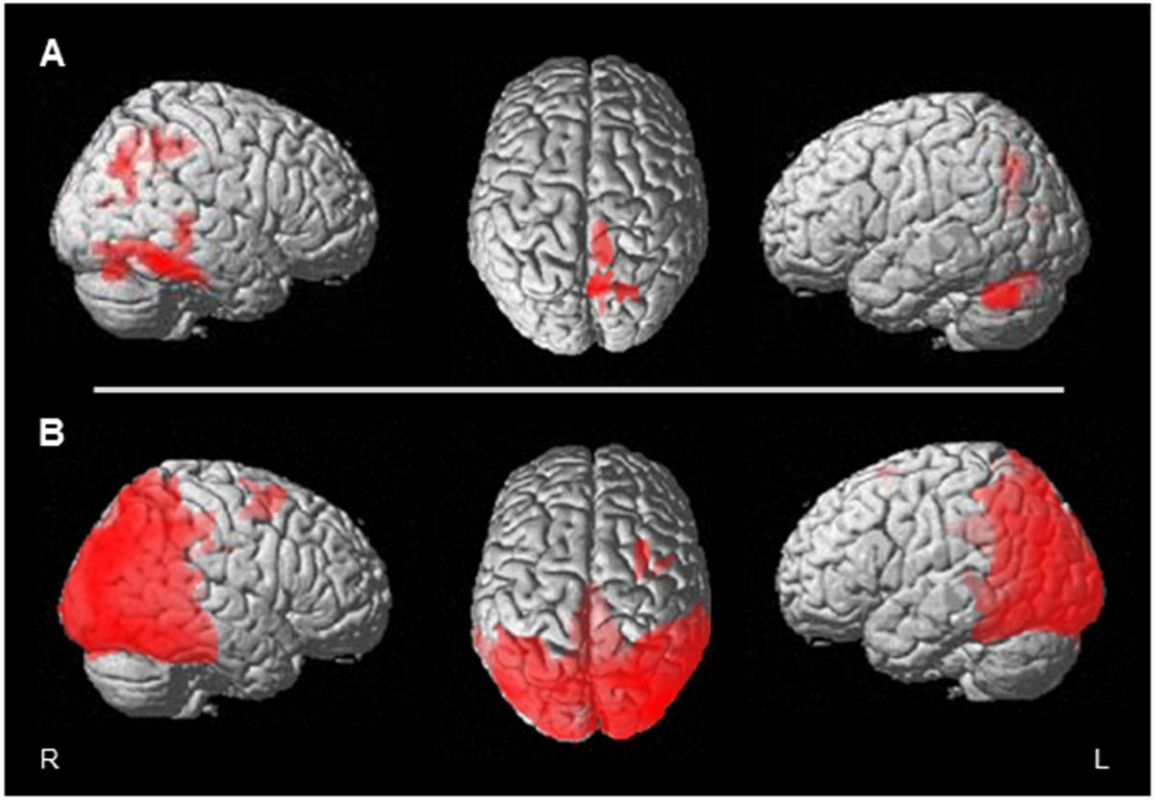

Figure 2. Tract-Based Spatial Statistics (TBSS) group maps ($p<0.05$, FWE corrected) of fractional anisotropy (FA), mode of anisotropy (MO), mean diffusivity (MD), axial diffusivity (AxD), and radial diffusivity (RD), displayed on axial view of the FMRIB standard-space FA template.

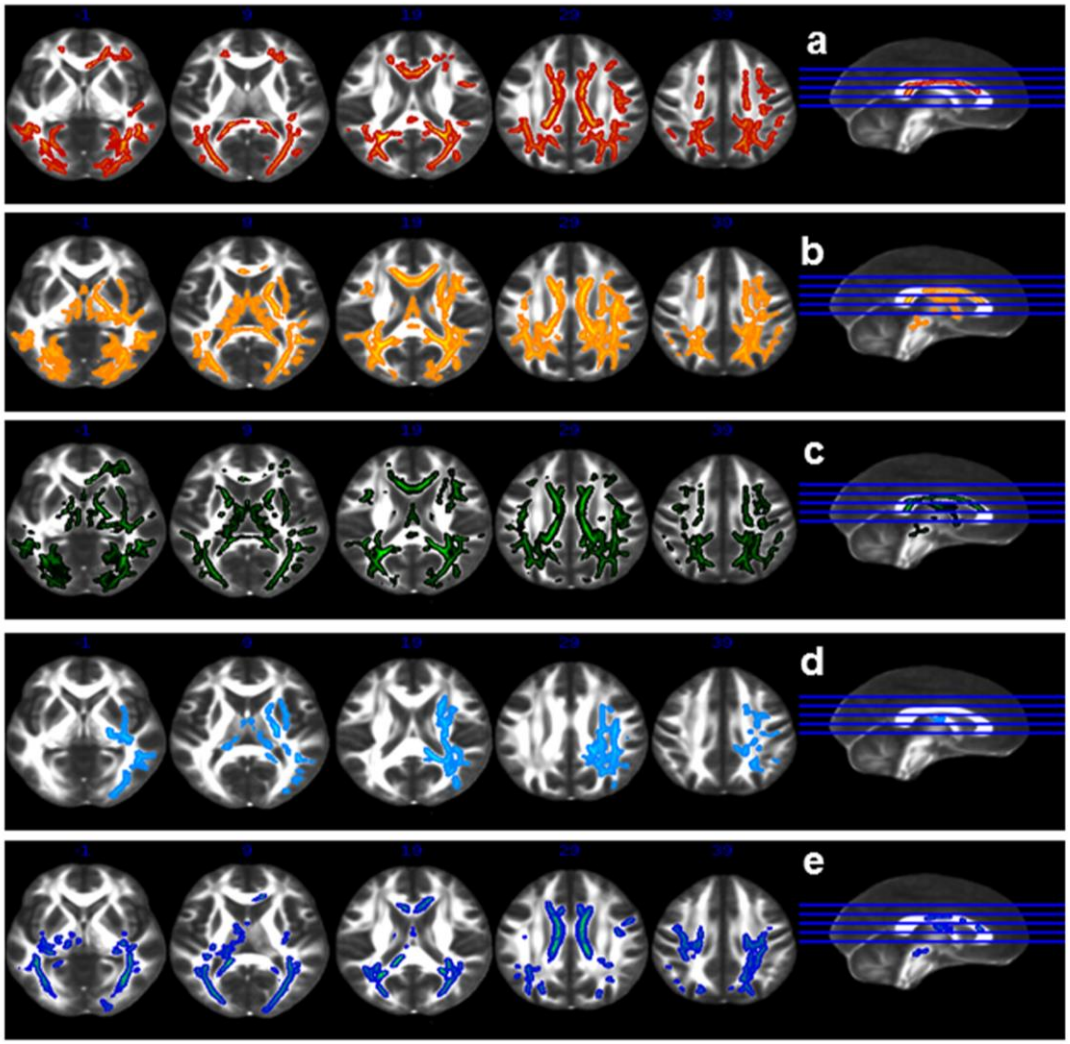

Figure 3. Objective voxel-based SPM-t [^{18}F]FDG-PET hypometabolic patterns of each PCA patient displayed on axial view of an MRI standardized structural scan ($p<0.05$, FWE corrected) showing bilateral temporo-parieto-occipital hypometabolism, and associated frontal involvement (see details in the text). SPM-t maps are displayed in a neurological convention (i.e., left = left; right = right) on a 5x5 matrix of transaxial images. Each axial slice covers 4 mms on the z-axis ranging from -40 to +56.

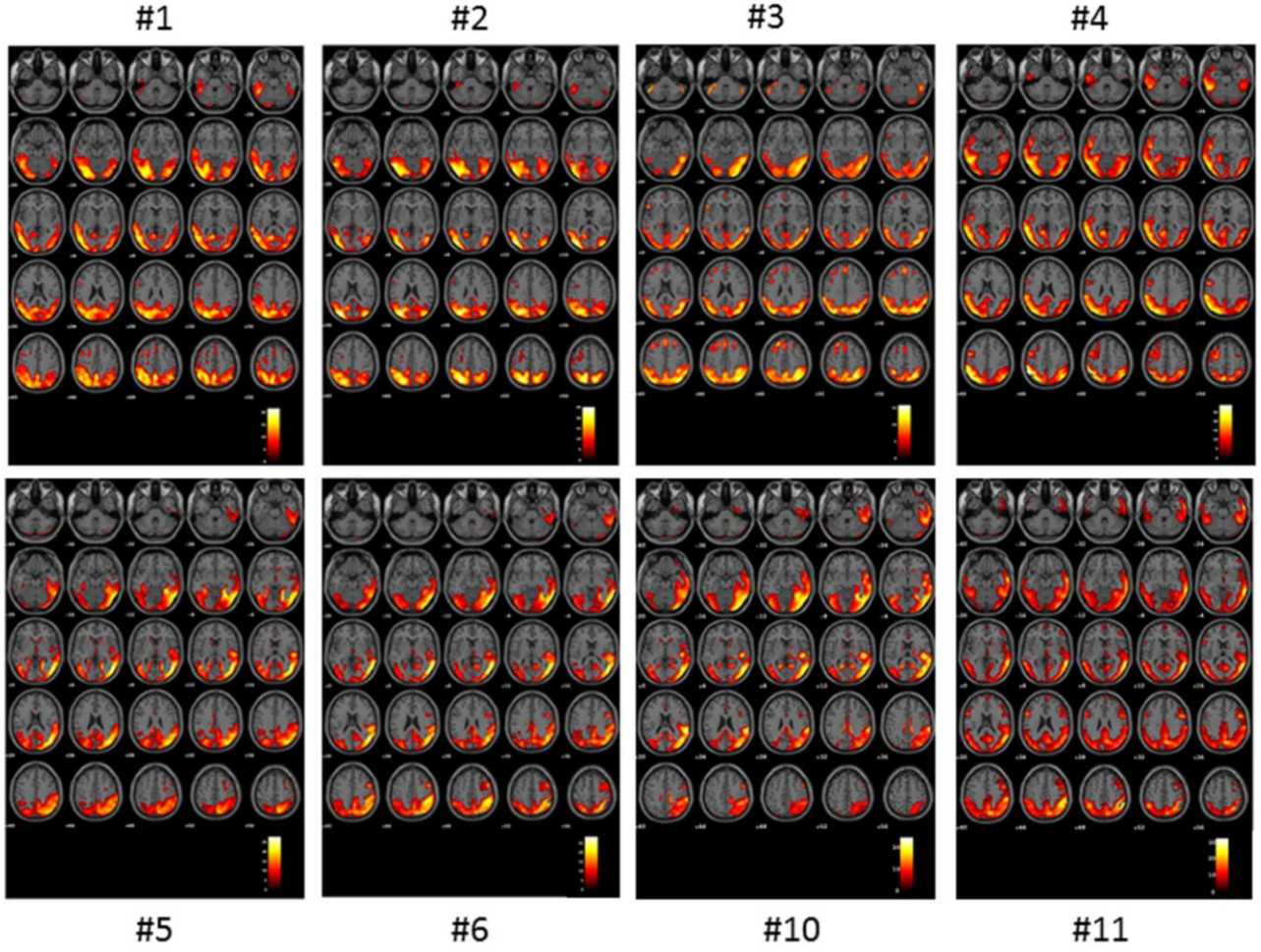

Supplementary Materials

Table 1. Summary of PET results : presence or absence of the involvement of specific brain regions in each patients and relative MNI coordinates of local maxima (x,y,z). H = Hemisphere; L = left; R = right.

Region	**H**	**# 1**	**# 2**	**# 3**	**# 4**	**# 5**	**# 6**	**# 7**	**# 8**	**# 9**	**# 10**
Middle Frontal Gyrus / precentral sulcus	L	-46 14 48	-24 2 62	-	-	-	-	-	-	-	-30 14 46
	R	30 20 62	-	28 36 42	38 -4 60	30 14 52	-	42 0 66	-	46 8 52	34 42 16
Superior Frontal Gyrus / superior frontal sulcus	L	-	-	-20 34 48	-	-	-20 2 70	-	-2 62 6	-	-18 58 4
	R	24 -4 72	-	24 14 66	-	24 2 74	-	26 14 68	8 62 24	20 -8 76	30 56 8
Middle Temporal Gyrus	L	-48 -68 16	-46 -66 10	-52 -54 18	-48 -68 18	-44 -66 12	-	-	-62 -50 6	-54 -64 16	-
	R	-	50 -70 6	50 -62 20	-	52 -68 4	50 -66 18	50 -66 18	62 -56 10	52 -56 8	52 -62 18
Superior Temporal Gyrus	L	-66 -40 18	-	-	-62 -40 18	-	-	-	-	-	-
	R	-	-	-	-	58 -28 14	58 -36 20	64 -38 22	-	-	-
Inferior Parietal Lobule	L	-48 -58 48	-56 -40 46	-32 -52 54	-52 -54 46	-	-	-	-46 -54 50	-	-34 -80 42
	R	-	16 -72 58	42 -48 44	-	46 -46 44	54 -42 46	44 -46 42	54 -50 48	54 -60 46	46 -48 48
Superior Parietal Lobule	L	-24 -60 66	-18 -68 54	-	-	-	-	-	-	-	-24 -54 72
	R	-	34 -56 60	32 -62 54	32 -54 66	30 -60 64	34 -56 60	-	32 -62 54	12 -74 52	32 -64 54
Fusiform Gyrus	L	-44 -48 -24	-28 -78 -14	-	-44 -54 -20	34 -48 -10	-	-	-	-	-
	R	-	-	24 -68 -12	-	-	30 -62 -6	36 -54 -10	-	-	32 -54 -10
Lingual Gyrus	L	-	-10 -80 -12	-	-32 -92 -16	-	-	-	-	-	-
	R	-	-	18 -80 -14	-	26 -62 -4	-	-	-	-	14 -56 4
Precuneus	L	-6 -50 76	-10 -54 54	-2 -62 46	-6 -70 58	-	-	-	-	-4 -64 40	-4 -54 14
	R	-	-	12 -74 54	-	12 -74 54	-	-	8 -54 38	8 -50 26	-
Cuneus	L	-6 -74 32	-6 -88 36	-4 -76 34	-	-	-	-	-	-	8 -90 28
	R		20 -68 38	10 -88 36	-	14 -98 24	10 -74 38	-	10 -74 38	10 -72 38	10 -74 38
Middle Occipital Gyrus	L	-28 -80 32	-44 -80 20	-38 -80 40	-36 -84 28	-28 -78 32	-	-	-46 -78 16	-	-32 -92 4
	R	-	42 -84 20	32 -86 20	-	32 -84 20	34 -92 -16	32 -84 20	-	-	48 -80 14
Inferior Occipital Gyrus	L	-36 -82 -12	-52 -64 -16	-	-50 -72 -4	-	-	-	-	-	-48 -68 -4
	R	-	38 -78 -14	36 -82 -16	-	48 -8 -12	46 -84 -14	46 -84 -14	44 -86 -14	44 -86 -16	38 -88 -16
Superior Occipital Gyrus	L	-26 -90 30	-20 -72 28	-	-18 -88 36	-	-	-	-	-	-
	R	-	-	24 -102 4	-	20 -72 38	-	-	-	-	16 -98 22
Calcarine Gyrus	L	-	-12 -64 16	-	-	-22 -68 10	-	-16 -56 10	-	-	-
	R	-	-	-	-	22 -66 8	-	-	-	12 -104 6	-